The solidification process of Al–Mg–Si alloys

Y. L. LIU
Institute of Metal Research, Chinese Academy of Sciences, Shenyang 110015, People's Republic of China

S. B. KANG
Korea Institute of Machinery and Materials, Changwon, 641-010, Korea

The microstructure and solidification process of three Al–Mg–Si alloys with different magnesium contents have been studied using optical microscopy and the electron probe X-ray microanalysis. The results showed that Al–Mg–Si alloys possessed fairly complicated solidification path: $L \rightarrow \alpha\text{-Al} + L_1 \rightarrow \alpha\text{-Al} + Al_{15}Si_2(FeMn)_3 + L_2 \rightarrow \alpha\text{-Al} + Al_{15}Si_2(FeMn)_3 + (\alpha\text{-Al} + Mg_2Si) + L_3 \rightarrow \alpha\text{-Al} + Al_{15}Si_2(FeMn)_3 + (\alpha\text{-Al} + Mg_2Si) + (\alpha\text{-Al} + Mg_2Si + Al_{15}Si_2(FeMn)_3)$, and wide solidification temperature of 75 °C. The magnesium content in the alloys greatly influenced the as-cast microstructure. The higher the magnesium content, the more Mg_2Si structure was present. Iron and manganese segregated to the finally solidified zone, which resulted in the formation of ternary eutectic structure. Although their content in the alloys was very low, their effect on solidification behaviour cannot be ignored.

1. Introduction

The demand for more lightweight, fuel efficient and enhanced performance automobiles stimulates the research and development of high-strength and high-formability aluminium alloys. The heat-treatable 6000 series Al–Mg–Si alloys, with medium to high strength, excellent formability and good corrosion resistance, possess great application potential in the automobile industry and have been subjected to extensive research [1–8]. A few new Al–Mg–Si alloys have been developed [9–11].

Magnesium and silicon are two basic elements in the 6000 series alloys to form Mg_2Si. Manganese was usually added to the alloys to form manganese-bearing dispersoids to retard the recrystallization. Iron is the main impurity in the alloys and forms deleterious intermetallic phases. The influence of alloying elements on microstructure and mechanical properties has been thoroughly investigated [2, 9, 12]. However, their effect on solidification process of alloys has received less attention. The solidification behaviour of binary Al–Mg alloys is relatively simple. After slowly solidifying, the alloys have a single-phase α-Al structure, even the content of magnesium in the alloys is quite high. While in the Al–Mg–Si alloys with less than 2 wt % Mg and less than 1 wt % Si, the as-cast microstructure is fairly complicated. It means that the addition of silicon has great influence on the solidification path of the alloys. It is of commercial interest to study the solidification process of the alloys and the formation of these intermetallic phases. The present study focused on the as-cast microstructure and solidification process of three magnesium-excess Al–Mg–Si alloys. The main purpose was to reveal the formation behaviour of non-equilibrium eutectic structure and coarse iron-bearing intermetallic phases.

2. Experimental procedure

Three alloys used in this study were prepared from high-purity aluminium, magnesium (99.99%) and Al–Si master alloy. The raw materials were air melted in a graphite crucible in an electrical resistance furnace and cast in a cast iron mould at 750 °C. The chemical compositions of the ingots were analysed by emission spectroscopy and are listed in Table I.

The investigation was carried out by remelting the alloys. The specimens, which were 10 mm × 10 mm × 30 mm in size, were cut from the ingots, homogenized and then heated to 750 °C in a graphite crucible in an air furnace. After being kept for 10 min at that temperature in order to melt the materials entirely and to homogenize the composition, the molten materials were then cooled in the furnace at a cooling rate of 2 °C min^{-1}. The solidification sequence of the alloys was investigated by a "water-quenching method" [13]. When the melt was cooled to a given temperature and a steady state had been reached by keeping the specimen at that temperature for 3 min, the specimen was dropped immediately into a water bath below the mouth of the furnace. The metallographic examination shows the solidification stage because liquid solidified during quenching is differentiated from the steady-state solidification products by its much finer microstructure. By quenching the specimen at different temperatures, the succeeding stages of solidification can thus be revealed and the solidification sequence determined. In order to determine the precipitation temperature of the eutectic structure and the final solidification temperature, relatively accurately, the quenching temperature intervals of 3 or 5 °C were taken in the final stage of solidification (575–550 °C).

The microstructure was analysed by optical microscopy and electronic microprobe. The specimens were

0022–2461

TABLE I The composition of the alloys (wt %)

Alloy	Mg	Si	Fe	Mn	Zr	Mg/Si
I	1.09	0.54	0.064	0.29	0.12	2.1
II	1.77	0.40	0.064	0.27	0.094	4.4
III	1.93	0.58	0.070	0.26	0.10	3.33

prepared by standard metallographic procedures and etched in a NaOH water solution. The electron probe analysis was done with a JAX-8600 electron probe X-ray microanalyser (EPMA) at an accelerating potential of 20 kV to determine all the compositions. In order to obtain a reliable value of the composition of the phases, the large-size phases were selected when performing EPMA analysis. The solid fractions at different temperatures were measured using a LECO-2001 imaging analysis system. The areal fraction was assumed to be equivalent to the volume fraction.

3. Results

3.1. The as-cast microstructure

Fig. 1 shows the as-cast microstructures of alloy II solidified at a cooling rate of 2 °C min^{-1}. It consisted of three phases: α-Al, Mg_2Si and $Al_{15}Si_2(FeMn)_3$. They were identified by a combination of morphology, EPMA analysis and etching characteristics. The α-Al phase formed the matrix of the material. Mg_2Si had two shapes: one possessed a lamellar or "Chinese script" characteristic, while the other was small blocky. The $Al_{15}Si_2(FeMn)_3$ phase also had two shapes: one was coarse blocky or "Chinese script", the other was small blocky. The comparatively coarse lamellar or "Chinese script" Mg_2Si and coarse blocky or Chinese script $Al_{15}Si_2(FeMn)_3$ were the products of binary eutectic reactions $L \rightarrow \alpha\text{-Al} + Mg_2Si$ and $L \rightarrow \alpha\text{-Al} + Al_{15}Si_2(FeMn)_3$, respectively, while the small blocky Mg_2Si and $Al_{15}Si_2(FeMn)_3$ were the products of ternary eutectic $L \rightarrow \alpha\text{-Al} + Mg_2Si + Al_{15}Si_2(FeMn)_3$. They formed at different solidification stages and were distributed at the grain boundary and interdendritic regions.

The compositions of the phases formed at different solidification stages were analysed by EPMA and are summarized in Table II. About Mg_2Si, the compositions of the constituents formed from the binary eutectic reaction (the lamellar) and the ternary eutectic reaction (the smaller block) are almost the same. But their stoichiometry deviated from the nominal composition of Mg_2Si. For $Al_{15}Si_2(FeMn)_3$, the small blocky shape resulting from the ternary eutectic reaction possessed slightly lower silicon and manganese contents than the coarse shape. Their stoichiometry

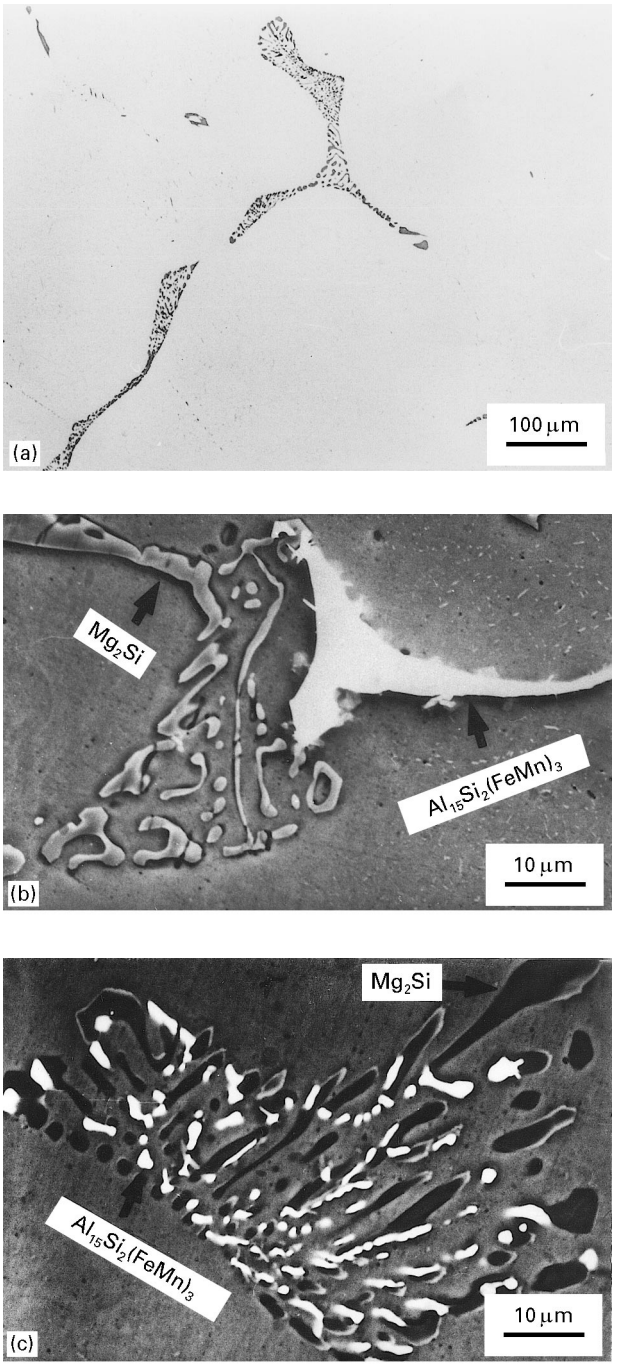

Figure 1 (a) The as-cast microstructure of alloy II. (b) The eutectic compounds Mg_2Si and $Al_{15}Si_2(FeMn)_3$. (c) The ternary eutectic structure (backscattered imaging).

TABLE II The compositions of the phases analysed by EPMA (at %)

Phase	Al	Mg	Si	Fe	Mn
Lamellar Mg_2Si	0	63.30	36.60	0.04	0.07
Small blocky Mg_2Si	0	63.23	36.76	0	0.02
Coarse blocky $Al_{15}Si_2(FeMn)_3$	75.21	0	5.74	12.07	6.97
Small blocky $Al_{15}Si_2(FeMn)_3$	78.63	0	4.58	11.95	4.84

[a] The results are the average of three measurements and no significant variation was observed among the measurements.

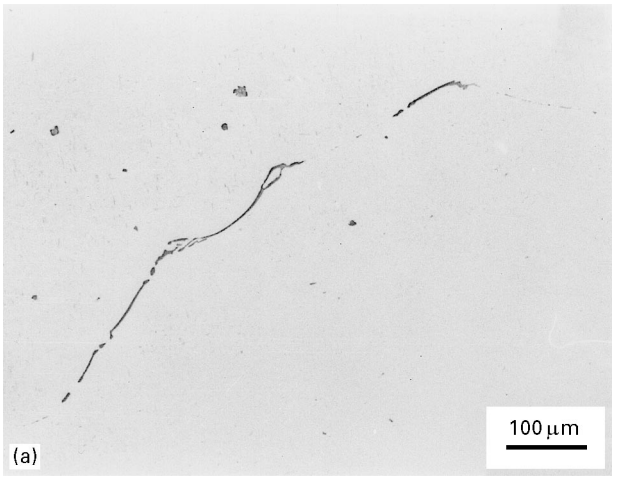

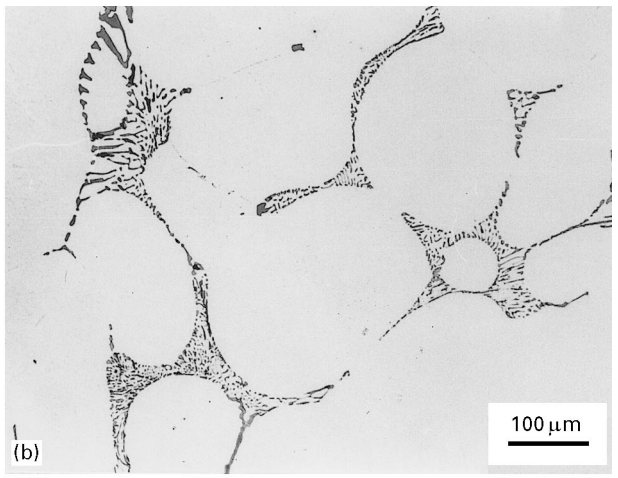

Figure 2 The as-cast microstructures of (a) alloys I and (b) III.

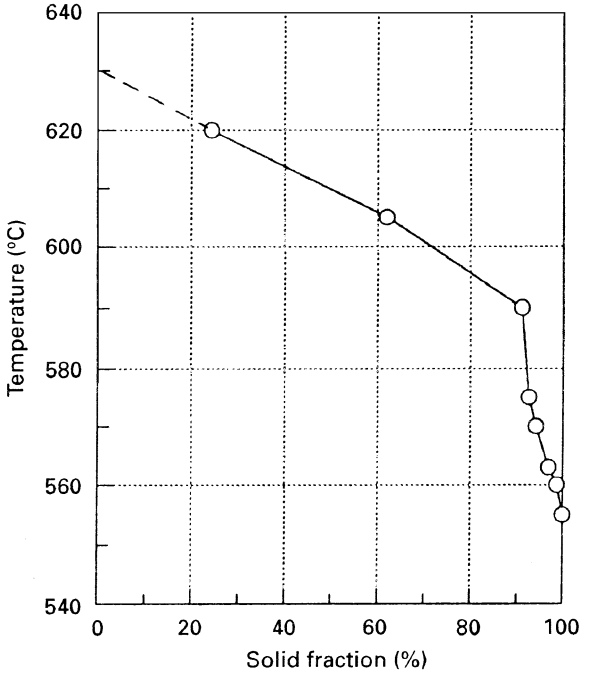

Figure 3 The fraction of solid versus temperature in alloy II.

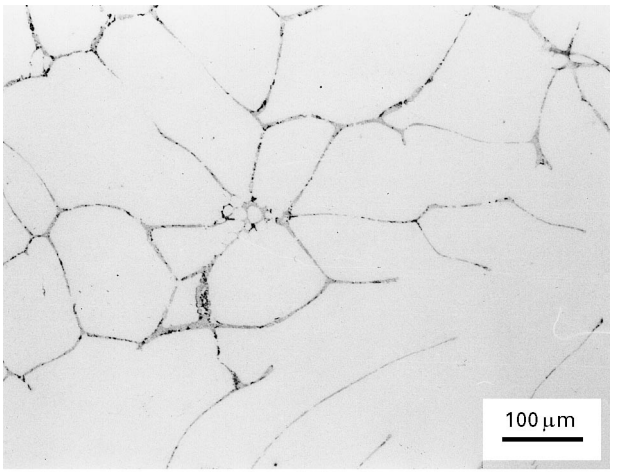

Figure 4 The remaining liquid of alloy II at 590 °C.

deviated from the nominal composition of the $Al_{15}Si_2(FeMn)_3$. These stoichiometry deviations resulted from the non-equilibrium eutectic reaction.

Fig. 2 shows the as-cast microstructures of the alloys I and III. In general, they consisted of α-Al matrix plus eutectic compounds. In alloy I, the eutectic structure Mg_2Si was much less than alloys II and III, it only existed in a few interdendritic regions. Moreover, the ternary eutectic structure is hard to find, while in alloy III, the fraction and size of Mg_2Si increased remarkably. From imaging analysis results, alloy II had 3.01% eutectic structure, alloy III had 4.76%. Obviously, they were influenced by both magnesium content and silicon content in the alloy. On the other hand, another intermetallic compound, coarse blocky or "Chinese script" $Al_{15}Si_2(FeMn)_3$ was almost the same in all three alloys, both in size and in volume fraction.

3.2. The solidification process of the alloys

Fig. 3 shows the relationship between solid fraction and temperature drop in alloy II. From Fig. 3, it can be inferred that the molten metal begins to solidify at about 630 °C. In the initial stage, the solidification rate was quite high. When the specimen was quenched into water from 590 °C, about 91% melt solidified, as shown in Fig. 4. However, with a further fall in temperature, the solidification rate became slower: at 575 °C, 7% melt still remained unsolidified, the solidified solid was still single α-Al, and the remaining liquid was enriched in several solutes, such as magnesium, silicon, iron and manganese. At about 570 °C, there was a new phase with coarse blocky or "Chinese script" structure, $Al_{15}Si_2(FeMn)_3$ precipitated from the remaining liquid, as shown in Fig. 5. As the temperature decreased further, no other new eutectic reaction occurred until 563 °C. The structure of the sample quenched from 563 °C was almost the same as that of the sample quenched from 570 °C. However, when quenching the specimen into water at 560 °C, the as-cast microstructure was very different from the former sample. In addition to $Al_{15}Si_2(FeMn)_3$, Mg_2Si with lamellar or "Chinese script" structure appeared, and a new complex structure formed: black blocks alternating with grey blocks, see Fig. 6. The grey one was

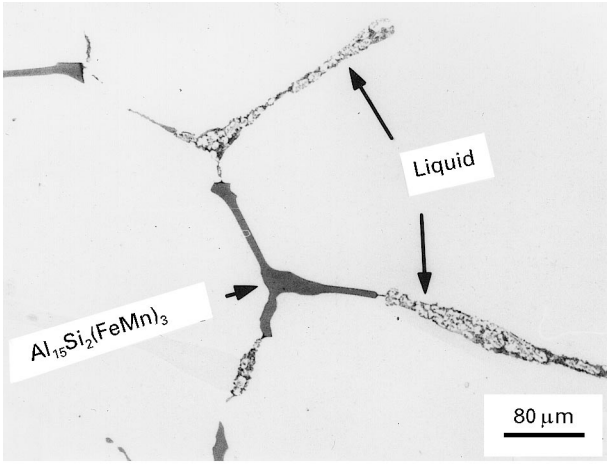

Figure 5 The precipitation of "Chinese script" $Al_{15}Si_2(FeMn)_3$ from the remaining liquid of alloy II at 570 °C.

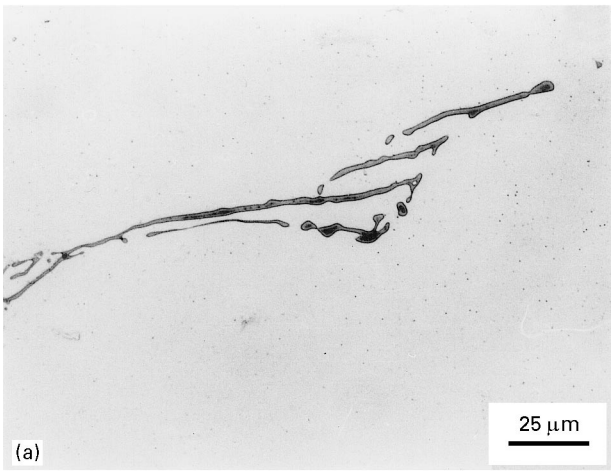

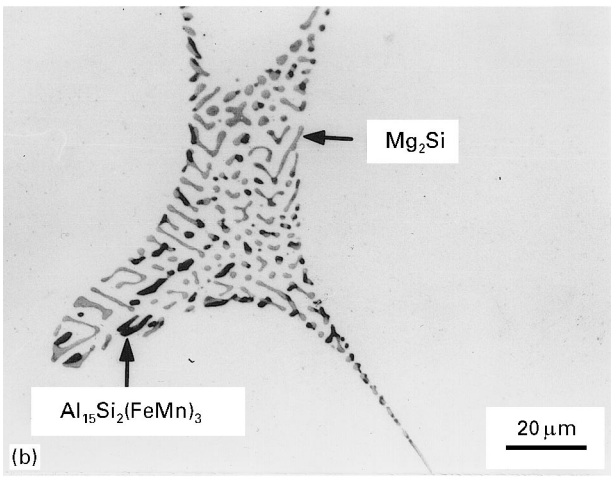

Figure 6 The constituents formed from the remaining liquid of alloy II: (a) binary eutectic α-Al + Mg_2Si; (b) ternary eutectic α-Al + Mg_2Si + $Al_{15}Si_2(FeMn)_3$.

Mg_2Si, while the black one was $Al_{15}Si_2(FeMn)_3$. It was the product of ternary eutectic. In addition, at this temperature, there still were a few unsolidified zones, see Fig. 7. These were enriched in magnesium, iron, silicon and manganese solutes. Finally, the solidification process terminated at about 555 °C. The solidification sequence of the alloy II was $L \rightarrow \alpha\text{-Al} + L_1 \rightarrow \alpha\text{-Al} + Al_{15}Si_2(FeMn)_3 + L_2 \rightarrow \alpha\text{-Al} + Al_{15}Si_2(FeMn)_3 + (\alpha\text{-Al} + Mg_2Si) + L_3 \rightarrow \alpha\text{-Al} + Al_{15}Si_2(FeMn)_3 + (\alpha\text{-Al} + Mg_2Si) + (\alpha\text{-Al} + Mg_2Si + Al_{15}Si_2(FeMn)_3)$.

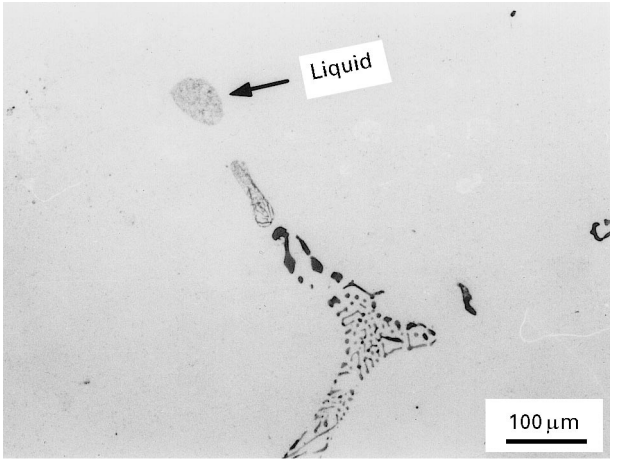

Figure 7 The unsolidified zone of alloy II at 560 °C.

A similar experiment was performed on alloys I and III. They possessed the same solidification path as in alloy II, and they also ended the solidification process at about 555 °C. The solidification temperature range was quite wide, about 75 °C.

4. Discussion

The as-cast microstructure and solidification process of Al–Mg alloy have been systematically studied [14]. It was found that in the case of slow solidification, the as-cast microstructure was single-phase α-Al, and no eutectic reaction occurred. The situation for the Al–Mg–Si alloys is very different. Under the conditions of slow solidification, the as-cast microstructure was quite complicated; not only binary eutectic structure, but also ternary eutectic appeared. This difference is attributed to the appearance of silicon, although its content was only in the range 0.4–0.58 wt %. On the one hand, the solute silicon possesses strong segregation tendency. During solidification, it was rejected to the front of the solid–liquid interface, which results in the concentration of silicon in the finally solidified zone reaching quite a high level. On the other hand, the addition of silicon promoted the segregation of solute magnesium. The high levels of magnesium and silicon in the finally solidified zone gave rise to the formation of eutectic compound Mg_2Si. From the Al–Mg–Si phase diagram [15], the solid solubility of magnesium in aluminium was reduced greatly by the appearance of silicon. In turn, the appearance of magnesium decreases the solid solubility of silicon in aluminium. For example, at the quasi-binary line, the solid solubility limit of magnesium and silicon in aluminium is 1.17 and 0.68 wt %, respectively (in the Al–Mg binary system, the solubility limit of magnesium in aluminium is 17.4 wt %, while in the Al–Si system, the solubility limit of silicon in aluminium is 1.65 wt %). The reduction of solid solubility of magnesium and silicon in aluminium gives rise to the easier formation of intermetallic compound Mg_2Si.

The other important factor influencing the as-cast microstructure is the magnesium concentration. From Table I, the difference in the content of silicon in the three alloys is not very large; alloy I has a higher silicon content than alloy II. The values of the Mg/Si ratio are all larger than 1.73, the nominal ratio of constituent Mg_2Si. However, the eutectic structure Mg_2Si in alloy I is much less than that of alloy II. This phenomenon is ascribed to the comparatively low magnesium content in alloy I. From the liquidus projection of the aluminium corner of the Al–Mg–Si system [15], at the two-fold saturation line of the eutectic reaction $L \rightarrow \alpha\text{-Al} + Mg_2Si$, the higher the magnesium content, the lower is the silicon composition. For the alloy with a low level of silicon, increasing the concentration of magnesium in the liquid is favourable for producing the eutectic structure of $\alpha\text{-Al} + Mg_2Si$. The solute magnesium possesses a relatively large redistribution coefficient. During solidification, its segregation tendency is comparatively small, which results in the lower magnesium concentration in the solid–liquid interface front. Increasing the magnesium content will result in a rising magnesium concentration at the interface front. Therefore, as for an alloy with a given silicon content, the higher the magnesium content, the easier it is for the eutectic structure to form.

The addition of manganese had a great influence on the constituent morphology of the iron-bearing phase. In the manganese-free Al–Mg–Si alloys, the iron-bearing phase is Al_5FeSi with plate structure [18], while in the manganese-containing Al–Mg–Si alloys used for this study, the morphology of the iron-bearing phase changed remarkably and its constituent became $Al_{15}Si_2(FeMn)_3$. In addition, the formation of small blocky $Al_{15}Si_2(FeMn)_3$ reduced the quantity of coarse blocky $Al_{15}Si_2(FeMn)_3$, which would be favourable for the improvement of mechanical properties.

In the solidification process of wrought aluminium alloys, there is a common characteristic: $L \rightarrow \alpha\text{-Al} + L_1$ is the main event during solidification. But the solidification behaviour of the finally solidified zone differs from each other. For the Al–Mg–Si alloys, the precipitation of primary phase α-Al rejected the solutes into the solid–liquid interface front, which gave rise to the increase in solute concentrations. Iron has strong segregation tendency, so that most of the iron atoms were concentrated in the remaining liquid. Although the iron content in the alloys was very low in the final solidificational stage its concentration would reach quite a high level. As soon as the eutectic composition was reached, an iron-bearing intermetallic phase precipitated. With the temperature falling further, and when the concentrations of magnesium and silicon in the residual liquid reached the eutectic point, eutectic structure Mg_2Si formed. Owing to the non-homogeneous segregation of solutes, some areas contained quite high concentrations of both magnesium and silicon, and iron and manganese. Therefore, the alloy had a lower final solidification temperature. Finally, the ternary eutectic reaction occurred and the solidification path terminated. From the solidification process of the alloys, it can be deduced that iron and manganese have great influence on the solidification process and as-cast microstructure. Although their content is very low, their effect cannot be ignored.

5. Conclusions

1. Al–Mg–Si alloys possessed fairly complicated solidification path: $L \rightarrow \alpha\text{-Al} + L_1 \rightarrow \alpha\text{-Al} + Al_{15}Si_2(FeMn)_3 + L_2 \rightarrow \alpha\text{-Al} + Al_{15}Si_2(FeMn)_3 + (\alpha\text{-Al} + Mg_2Si) + L_3 \rightarrow \alpha\text{-Al} + Al_{15}Si_2(FeMn)_3 + (\alpha\text{-Al} + Mg_2Si) + (\alpha\text{-Al} + Mg_2Si + Al_{15}Si_2(FeMn)_3)$, and a wide solidification temperature of 75 °C.

2. The magnesium content in the alloys greatly influenced the as-cast microstructure. The higher the magnesium content, the more Mg_2Si structure was present. In the high magnesium alloys, not only binary eutectic structure, but also ternary eutectic structure formed.

3. Iron and manganese segregated to the finally solidified zone and produced a complex intermetallic compound $Al_{15}Si_2(FeMn)_3$ as well as ternary eutectic structure. Although the iron content in the alloys was very low, its effect on solidification should not be ignored.

References

1. A. K. GUPTA, G. B. BURGER, P. W. JEFFREY and D. J. LLOYD, in "Proceedings of the 4th International Conference on Aluminium Alloys", Vol. 2, edited by T. H. Sanders Jr and E. A. Starke Jr (Georgia Institute of Technology, Atlanta, 1994) p. 187.
2. W. S. MILLER, J. BOTTEMA, N. RAGHUNATHAN and R. GRIMBERGEN, *ibid*., Vol. 1, p. 410.
3. B. THANABOONSOMBUT and T. H. SANDERS Jr, *ibid*., Vol. 2, p. 197.
4. S. A. COURT, H. D. DUDGEON and R. A. RICKS, *ibid*., Vol. 1, p. 395.
5. DAN ZAO and P. K. CHAUDHURY, *ibid*., Vol. 1, p. 426.
6. G. J. MARSHALL, A. J. E. FLEMMING, A. GRAY and R. LLEWELLYN, *ibid*., Vol. 1, p. 467.
7. S. J. ANDERSEN, *Metall. Trans.* **26A** (1995) 1931.
8. Q. WU and S. B. KANG, *Scripta Met. Mater*., to be published.
9. S. J. MURTHA, "New 6xxx aluminium automotive body sheet applications", presented at the 1995 SAE International Conference, SAE Technical Paper Series 950718.
10. S. C. BERGSMA and M. E. KASSNER, in "Proceedings of the 4th International Conference on Aluminium Alloys", Vol. 3, edited by T. H. Sanders Jr and E. A. Starke Jr (Georgia Institute of Technology, Atlanta, 1994) p. 187.
11. S. C. BERGSMA and M. E. KASSNER, *ibid*., Vol. 1, p. 403.
12. T. SAKURAI and T. ETO, in "Proceedings of the 3rd International Conference on Aluminium Alloys", Vol. 1, edited by L. Arnberg, O. Lohne, E. Nes and N. Ryum (Norwegian Institute of Technology/SINTEF, Trondheim, 1992) p. 208.
13. Y. L. LIU, Z. Q. HU, Y. ZHANG and C. X. SHI, *Metall. Trans.* **24B** (1993) 857.
14. Y. L. LIU and S. B. KANG, *Mater. Sci. Tech.* **12**(1) (1996) 12.
15. L. F. MONDOLF, "Aluminium Alloys: Structure and Properties" (Butterworth, London, 1976) p. 567.

Received 23 February
and accepted 31 July 1996